

# Assessing the Potential of MODIS/Terra Acquired Thermal Imagery in De- tecting and Monitoring Coal Fires

a contribution to the joint coal fire research initiative:

*"Reception and project specific processing of remote sensing data for the support of current and future projects within the Chinese-German environmental research co-operation"*



CHRIS HECKER  
DEPARTMENT OF EARTH SYSTEMS ANALYSIS  
INTERNATIONAL INSTITUTE FOR GEO-INFORMATION SCIENCE AND EARTH OBSERVATIONS (ITC)  
ENSCHEDÉ, THE NETHERLANDS  
NOVEMBER 2003

## **Abstract**

**Coal fires are a major problem in many coal producing countries. Remote sensing is an efficient and economic way to detect and monitor those coal fires over large areas. For several years the Landsat group of sensors has given good results for detecting coal fires. Recent problems with Landsat7's optical system requires the user community to search for alternative sensors.**

**This work looks at the possibilities MODIS images offer in the field of coal fire detection and monitoring for a study area in north-central China. Day and night images of different seasons are compared and various band ratios assessed.**

**The document will show that night images of MODIS scenes can be used to detect coal fires even if the fires are only a fraction of the pixel size in the image. Best results are achieved when ratioing winter night image bands 20 and 32.**

**With two MODIS sensors currently circling the globe, two day and two night images are acquired per day. Compared to other earth observing sensors, where night images are hard to come by, MODIS offers the opportunity to base a whole monitoring programme on night images alone.**

**As MODIS data are available free of charge, MODIS images have a great potential for regular regional monitoring of coal fires even in lesser developed countries.**

## TABLE OF CONTENTS

1. Introduction .....	1
1.1. MODIS Background.....	1
1.2. Problem Definition and Justification.....	1
1.3. Research Question and Approach .....	2
2. Materials.....	3
2.1. Study Area.....	3
2.2. Data Sets.....	3
2.2.1. MOD021K.....	4
2.2.2. MOD03.....	4
2.2.3. Ground Survey Information .....	4
2.3. Software .....	4
3. Preprocessing .....	4
3.1. Bowtie correction .....	4
3.2. Import into ENVI .....	5
3.3. Georeferencing .....	5
3.4. Reprojection to UTM Grid .....	5
4. Data Processing .....	6
4.1. Brightness Temperatures .....	6
4.2. Band Ratioing.....	6
4.3. Principal Components and Minimum Noise Fraction .....	8
4.4. Day/Night Pair Calculations.....	8
4.5. Maximum vs. Average .....	8
5. Results and Discussion.....	9
5.1. Brightness Temperature Results.....	9
5.2. Band Ratioing Results.....	10
5.3. PC and MNF Results.....	12
5.4. Day/Night Pair Results.....	13
5.5. Maximum vs. Average Results.....	14
6. Conclusions and Recommendations.....	15
7. Acknowledgements .....	17
8. References .....	17
9. Appendices .....	18
9.1. Appendix A .....	19
9.2. Appendix B .....	20
9.3. Appendix C .....	21
9.4. Appendix D .....	23

## LIST OF FIGURES

Figure 1 MODIS day time Band20 showing the study areas. The dark, linear feature is the Yellow River flowing towards the top of the figure. ....	3
Figure 2 Blackbody curves of 1% coal fires at 450K, 99% background at 273K and linear mixture of both. In navy-blue the location of MODIS TIR bands. ....	7
Figure 3 Mean brightness temperature values for entire scene. Band number 1-16 corresponds with MODIS bands 20-36 (without 26). Bands with reduced mean temperatures are influenced by atmospheric absorptions. ....	7
Figure 4 MODIS band 20 day images; a) summer day time scene of August 29, 2002 with vegetated areas showing up in dark along the Yellow River valley; b) winter day time scene of February 12, 2003. Both images linearly stretched on the zoom window. ....	10
Figure 5 MODIS band 20 night time images; a) summer night time scene of August 29, 2002 with the eastern slopes of the Helan Shan (east of Ruqigou study area) still hot from the day; b) winter day time scene of February 12, 2003. Solar heating effects are still visible but less pronounced than during summer. Both images linearly stretched on the zoom window. ....	10
Figure 6 MODIS band ratio 23/32 day images; a) the summer day time scene of August 29, 2002 shows no results; b) the winter day time scene of February 12, 2003 reveals a hot spot just left below centre and in the top right corner. Both images linearly stretched on the zoom window. ....	11
Figure 7 MODIS band ratio 20/32 night images; a) the summer night time scene of August 29, 2002 shows the Ruqigou fires clearly as well as a hot spot in the northeast quadrant of the zoom window; b) the winter night scene of February 12, 2003 shows even better contrasts; other hot spots southeast of Wuda along the Yellow River are heat sources from industry Both images linearly stretched on the zoom window. ....	12
Figure 8 Comparison of MODIS band ratio 20/32 night images; a) winter night scene of March 18, 2002. Distinction between fires and background is difficult; b) the comparable winter night scene of February 12, 2003 clearly shows the fires, industrial hot spots and the Yellow River. Both images 2% linearly stretched on the zoom window. ....	12
Figure 9 Comparison of MODIS day/night calculation with a single night scene ratio; a) day/night combination according to formula Try3. Two industrial hot spots are visible along the right edge of the zoom window; b) the 20/32 band ratio of the same days night scene shows the hot spots much clearer. Both images from February 12, 2003 and 2% linearly stretched on the zoom window. ....	13
Figure 10 Comparison of resampling weight setting; a) average weighting smoothens background as well as hot spots; b) maximum weighting gives good detection contrast but may exaggerate the temperature contrast and size of the actual fire area. Both images from March 18, 2002 and linearly stretched on the zoom window. ....	14

## LIST OF TABLES

Table 1 MODIS band numbering and attributes (from ITC's Sensor Database; <a href="http://www.itc.nl/research/products/sensordb/searchsat.aspx">http://www.itc.nl/research/products/sensordb/searchsat.aspx</a> ).....	2
--	---

## LIST OF ACRONYMS AND ABBREVIATIONS

DFD	German Aerospace Center
DLR	German Remote Sensing Data Center
EOS	Earth Observing System program (NASA)
ETM+	Enhanced Thematic Mapper Plus (Landsat7 sensor)
IIFOV	Instantaneous Field of View
ITC	International Institute of Geo-Information Science and Earth Observation, The Netherlands
MNF	Minimum Noise Fraction (related to PC)
MODIS	Moderate Resolution Imaging Spectroradiometer
NASA	National Aeronautics and Space Administration, USA
PC	Principal Components

# 1. Introduction

## 1.1. MODIS Background

The Moderate Resolution Imaging Spectroradiometer (MODIS) is a spaceborne imaging instrument that was first launched by NASA on the Terra satellite platform in 1999. Since 2002 an identical MODIS instrument has been operational on NASA's Aqua satellite. Since then, the two instruments have delivered images in 36 spectral bands ranging from the visible wavelengths up to the Thermal Infrared (TIR). The repeat cycle of the sun-synchronous platforms is 16 days but due to the large swath width of over 2000 km, each area can be imaged every 1-2 days. Since the thermal bands are an integral component of the MODIS instrument and product system, the satellite is routinely left turned on during its ascending (i.e. night) half of its orbits.

Spatial resolution is relatively low with 1 km in all bands; although a selection of the higher frequency bands is also available at 250 and 500m respectively (Table 1).

The radiometric resolution of 16 bits is quite high, allowing for the detecting of even small temperature differences in the TIR bands.

## 1.2. Problem Definition and Justification

Coal fires are a major problem in many coal-producing countries. Fires can occur on the surface at coal seam outcrops as well as in coal stock piles and waste piles. Other fires are burning underground with a variable amount of overburden rocks in between the fire and the surface.

For a more detailed account on the coal fire problem, the reader is referred to (Rosema et al., 1999).

To tackle the coal fires properly, it is essential to detect their location as early as possible. Following their detection, checks on a regular basis are needed to monitor their development as well as to assess the efficiency of coal fire fighting efforts.

Many studies have shown that remote sensing is a suitable tool for detecting as well as monitoring coal fires (Rosema et al., 1999; Zhang, Wagner, Prakash, Mehl, & Voigt, 2003). One of the most successfully used spaceborne sensors for coal fire detection, was Landsat 7's ETM+ and the earlier versions of the Landsat family.

Recently, the ETM+ sensor has developed a problem with a moving part of its optical system. Images after May 2003 are only partly useful. With ETM+ being partly out of commission, the remote sensing user community has to look around for alternative sensors. MODIS' thermal bands could be an alternative for ETM+ in coal fire monitoring.

**Table 1 MODIS band numbering and attributes (from ITC's Sensor Database; <http://www.itc.nl/research/products/sensordb/searchsat.aspx>)**

<b>Band</b>	<b>Wavelength [<math>\mu\text{m}</math>]</b>	<b>Resolution [m]</b>	<b>Swath Width [km]</b>
Band 1 (VIS)	0.62 to 0.67	250	2330
Band 2 (NIR)	0.841 to 0.876	250	2330
Band 3 (VIS)	0.459 to 0.479	500	2330
Band 4 (VIS)	0.545 to 0.565	500	2330
Band 5 (NIR)	1.23 to 1.25	500	2330
Band 6 (SWIR)	1.628 to 1.652	500	2330
Band 7 (SWIR)	2.105 to 2.155	500	2330
Band 8 (VIS)	0.405 to 0.42	1000	2330
Band 9 (VIS)	0.438 to 0.448	1000	2330
Band 10 (VIS)	0.483 to 0.493	1000	2330
Band 11 (VIS)	0.526 to 0.536	1000	2330
Band 12 (VIS)	0.546 to 0.556	1000	2330
Band 13 (VIS)	0.662 to 0.672	1000	2330
Band 14 (VIS)	0.673 to 0.683	1000	2330
Band 15 (VIS)	0.743 to 0.753	1000	2330
Band 16 (NIR)	0.862 to 0.877	1000	2330
Band 17 (NIR)	0.89 to 0.92	1000	2330
Band 18 (NIR)	0.931 to 0.941	1000	2330
Band 19 (NIR)	0.915 to 0.965	1000	2330
Band 20 (MWIR)	3.66 to 3.84	1000	2330
Band 21 (MWIR)	3.929 to 3.989	1000	2330
Band 22 (MWIR)	3.929 to 3.989	1000	2330
Band 23 (MWIR)	4.02 to 4.08	1000	2330
Band 24 (MWIR)	4.433 to 4.498	1000	2330
Band 25 (MWIR)	4.482 to 4.549	1000	2330
Band 26 (SWIR)	1.36 to 1.39	1000	2330
Band 27 (TIR)	6.535 to 6.895	1000	2330
Band 28 (TIR)	7.175 to 7.475	1000	2330
Band 29 (TIR)	8.4 to 8.7	1000	2330
Band 30 (TIR)	9.58 to 9.88	1000	2330
Band 31 (TIR)	10.78 to 11.28	1000	2330
Band 32 (TIR)	11.77 to 12.27	1000	2330
Band 33 (TIR)	13.185 to 13.485	1000	2330
Band 34 (TIR)	13.485 to 13.785	1000	2330
Band 35 (TIR)	13.785 to 14.085	1000	2330
Band 36 (TIR)	14.085 to 14.385	1000	2330

### 1.3. Research Question and Approach

This study tries to assess the usefulness of MODIS/Terra derived images, in detecting coal fire related hot spots.

For that purpose, MODIS images from the DLR archive as well as from NASA's EOS Data Gateway (<http://edcimswww.cr.usgs.gov/pub/imswelcome/>) were analysed and compared visually to known coal fire locations surveyed during the 2002 and 2003 field visits.

It is beyond the scope of this study to develop an algorithm for an automatic detection of the hot spots based on the MODIS imagery. This study also deals with MODIS/Terra acquired data only. No MODIS/Aqua data are included in this study.

## 2. Materials

### 2.1. Study Area

The study area for this investigation lies in north-central China. The two mining sites are in Wuda and Ruqigou. They are located in the Inner Mongolia and Ningxia Hui Autonomous Regions, respectively. The locations differ in several physical aspects. Wuda is located at the edge of the Gobi desert and at about 1200 m altitude, it lies just above the valley of the Yellow River. Most of the fires in the area are underground fires with only small areas showing temperatures distinctly above background values. Ruqigou is situated in the Helan Shan mountains with altitudes ranging around 2000 m. Many of the coal seams are burning at the surface and create more distinct surface temperature anomalies than in Wuda.

The approximate location of the Wuda coal fields is 39.5°N 106.6°E; Ruqigou's coal fields are situated at 39.1°N 106.1°E.

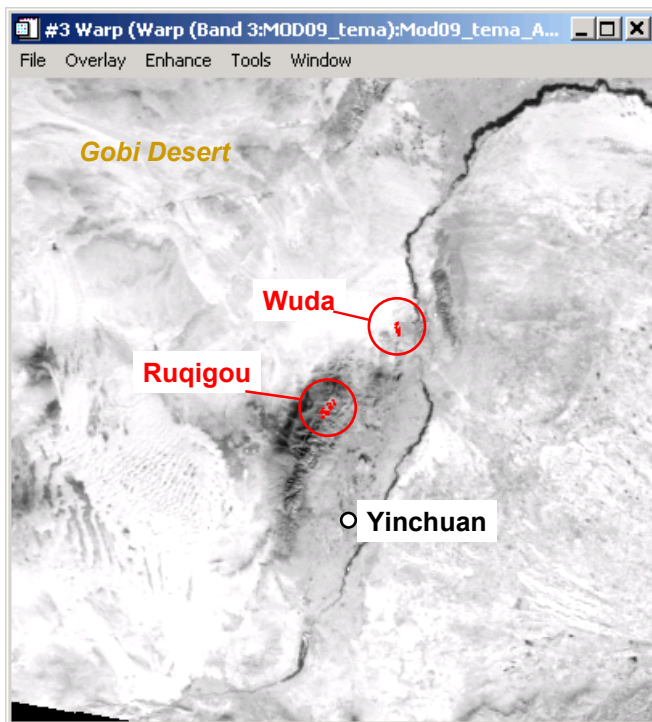


**Figure 1** MODIS day time Band20 showing the study areas. The dark, linear feature is the Yellow River flowing towards the top of the figure.

### 2.2. Data Sets

Apart from the actual imagery, the MODIS science team has developed many different higher-level data products. To differentiate between the various data types, a product identifying code is put at the beginning of all file names. MODIS/Terra data start with *MOD* followed by a two-digit product code. MODIS/Aqua data sets can be easily differentiated as their file names start with *MYD*.

The table in Appendix A shows the data sets acquired during this study.

### 2.2.1. MOD021K

The MOD021K data are the Level 1B processed image data at 1 km spatial resolution. Apart from the actual imagery data, it also contains basic geolocation information inside the hdf file structure. This product is the main image type analysed in this study.

### 2.2.2. MOD03

MOD03 is a MODIS geolocation collection that contains geodetic latitude and longitude information, altitude values above geoid as well as a land/sea mask. This file type was used to replace the more rudimentary geolocation information inside the MOD021K file during bowtie correction and georeferencing. A separate MOD03 file exists for each MOD021K image.

### 2.2.3. Ground Survey Information

During the September 2002 joint fieldwork between DLR and ITC the extent of the coal fire related surface temperature anomalies were mapped in Wuda and Ruqigou coal mining areas. A vector file containing the information collected during the fieldwork was used to compare the outcome of the MODIS processing with known fire locations.

## 2.3. Software

Most of the work was done with the help of ENVI 3.6. This is a commonly used, off-the-shelf image processing software. It offers the advantages of handling multi-band data very well and offers great flexibility when using IDL-based scripting for some of the operations.

The bowtie correction is done by the help of a freeware tool called MS2GT (MODIS Swath-to-Grid Toolbox; <ftp://sidacs.colorado.edu/pub/NSIDC/>). It consists of a combination of PEARL scripts and IDL routines. While developed for UNIX systems, it was possible to tweak some of the shell files to make them run properly on a LINUX operating system as well.

A java-based executable was developed to create a ground control point file for georeferencing the images. It takes latitude and longitude output files of the MS2GT and puts them into an ENVI readable format.

# 3. Preprocessing

## 3.1. Bowtie correction

To achieve the over 2000m wide swath width, MODIS uses a whiskbroom scanner with a maximum scan angle of 55° to either side of the flight line. This very large scan angle causes the instantaneous field of view (ifov) to increase from 1x1 km at nadir to almost 2x5 km at maximum scan angle. This increase in ifov produces an overlap of adjacent scan lines, which then causes a repetition of features in the image at every 10<sup>th</sup> scan line. This is often referred to as the Bowtie Effect and for proper results, corrections have to be applied to restore the original geometry.

A commonly used tool to correct for the Bowtie Effect is the MODIS Swath-to-Grid Toolbox (MS2GT; compare chapter 2.3). It allows the user to output the bowtie corrected image to a gridded floating point ASCII file. During the correction process, adjacent scenes can be glued, geolocation information is read from a MOD03 file and brightness temperatures can be calculated. For a full account of the possibilities of the MS2GT, the reader is referred to the website <http://nsidc.org/PROJECTS/HDFEOS/MS2GT/>.

In this study, the following parameters were used for the MS2GT:

- Input files:* MOD021K and its corresponding MOD03 geolocation file
- Output files:* Bands 20-25 and 27-36(in brightness temperature); solar zenith angle, sensor zenith angle; geolocation files (reading for each output pixel)
- Output grid:* 800 cols; 600 rows; 1x1 km; Azimuthal EA projection; (also see Ninxia.mpp and Ninxia.gpd in Appendix C for details)
- Weight type:* By default, pixel values are *Averaged* during the resampling; to test if averaging results in lower detectability, two scenes were reprocessed using a *Maximum* weight type
- Output format:* Floating point ASCII files

It appears that ERDAS Imagine's MODIS import as well as some IDL-based tools developed by the ENVI user community may allow similar corrections directly inside these popular remote sensing software packages (Personal Comm. J. Kooistra, ITC). The options and the quality of the results are not yet known to the author.

### **3.2. Import into ENVI**

To display the bowtie corrected images, an ENVI header file was created. Since all output images are based on the identical grid, the header information can be copied to all files to be imported into ENVI. Bands of the same scene were then stacked into proper ENVI files.

### **3.3. Georeferencing**

At this point in the processing the ENVI files created had no projection information yet. This is changed by assigning an ENVI ground control point file (ninxia\_lon\_lat\_ascii.pts). The information in this file came from the MS2GT geolocation output and was modified into an ENVI-readable format with the help of a short Java-based programme.

### **3.4. Reprojection to UTM Grid**

All files were further resampled into a 1x1 km grid based on WGS84 datum and UTM Zone 48. This allows for an easy comparison of the output with existing images of other sensors as well as with results of the ground-based surveys.

## 4. Data Processing

### 4.1. Brightness Temperatures

During the bowtie correction the raw digital number values were already transferred into calibrated Brightness Temperatures. Hence, the images could be directly analysed for anomalous brightness temperature levels near known coal fire locations. To achieve the best temperature contrasts, the images were stretched temporarily (local linear or linear 2% stretch).

### 4.2. Band Ratioing

As of the beginning of the study, it was expected that band ratios would give better results than brightness temperatures alone. With a pixel size of 1x1 km, all coal fires will only take up part of the area sensed by the MODIS sensor at any given time. Therefore, the resulting temperature will, be a mixture of background temperatures and the coal fires themselves. If we assume linear mixing of two different temperatures making up the sensed pixel (Dozier, 1981), the contribution of the hot fires in the shorter wavelengths will be relatively greater than in the longer wavelengths. While these contributions may not be significant enough to stand out properly in the brightness temperature images, a ratio of shorter and longer TIR wavelengths should produce better results.

In order to decide which wavelengths should be used, a conceptual model was developed; estimating fire size as well as fire and background temperatures.

The background temperature will, of course, vary, but for a night time, winter acquisition can be estimated at 273 K for the target area.

Field surveys showed, that typical surface temperatures over strong, coal fire related temperature anomalies lay around 400-500 K.

In each fire pixel, the actual fire only takes up a certain fraction of the instantaneous field of view. For this model, 1% is assumed to have temperatures at 400-500 K.

The choices made above are estimations based on field experience. The model has yet to be validated with the remotely sensed data. For illustrating the principle of band ratioing and selecting bands, the accuracy of the conceptual model is sufficient.

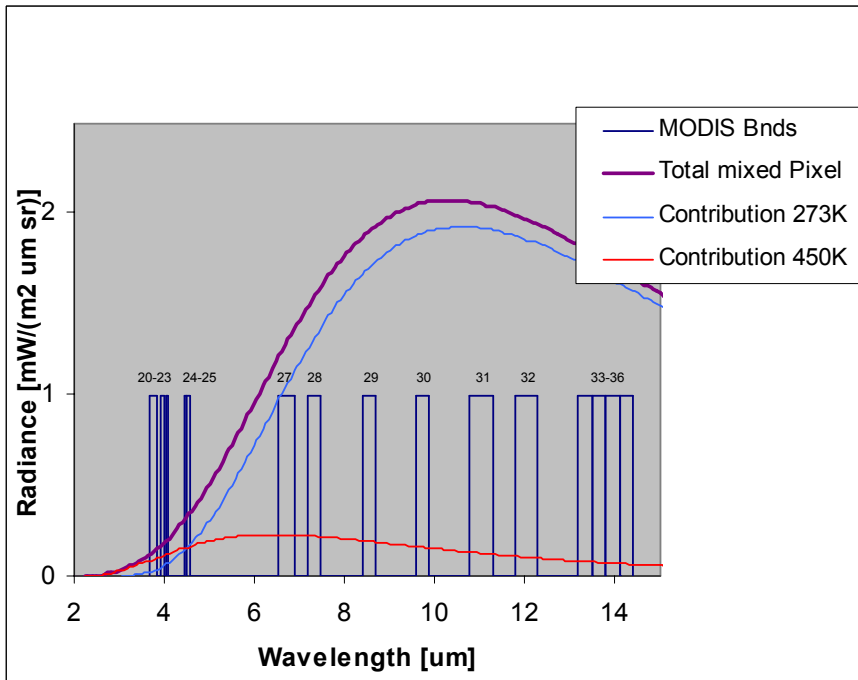


**Figure 2** Blackbody curves of 1% coal fires at 450K, 99% background at 273K and linear mixture of both. In navy-blue the location of MODIS TIR bands.

Another important aspect to consider is the position of the bands compared to atmospheric windows; bands 24, 25 and 33-36 are attenuated by CO<sub>2</sub>, bands 27 and 28 by water vapour and band 30 by O<sub>3</sub>. These bands are often showing considerable striping and relatively small contrast. The effect of the absorbing gases can also be demonstrated by looking at the brightness temperatures in various bands. Wavelengths that encounter strong absorption will show reduced temperatures.

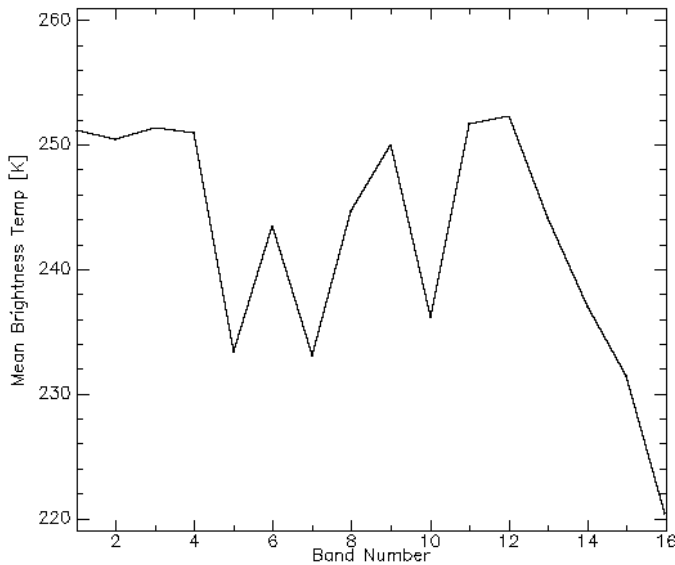


**Figure 3** Mean brightness temperature values for entire scene. Band number 1-16 corresponds with MODIS bands 20-36 (without 26). Bands with reduced mean temperatures are influenced by atmospheric absorptions.

Since band 21 and 22 cover the same wavelength, we can also exclude the less sensitive band 21. The remaining bands are 20, 22, 23, 29, 31 and 32. Including also the information from the blackbody curves of the conceptual model above, ratios between the lower (20-23) and higher group (29-32) of bands should give useable results.

The actual ratios are calculated from the brightness temperature files. The outputs are floating point files with values grouping around value 1. Since in TIR images higher temperatures are usually represented by lighter colours, the numerator and denominator were selected in a way to give coal fire pixels higher values than surrounding background. To achieve the best temperature contrasts, the images were stretched temporarily (local linear or linear 2% stretch).

Appendix B shows the ratios analysed.

### 4.3. Principal Components and Minimum Noise Fraction

Principal Components (PC) and Minimum Noise Fraction (MNF) rotations were carried out on selected night time files. First on brightness temperatures and later on the ratios as well. As first results were not very promising, the processing was halted after a few files.

### 4.4. Day/Night Pair Calculations

Day time surface temperatures are strongly influenced by solar heating and overprint the small influences of the underlying coal fires completely. While the background temperatures vary a lot as the day progresses, the radiation contribution of the fires should stay more or less stable. Therefore, an attempt was made to compare day/night image pairs to resolve the pixels with underlying coal fires.

Day/night ratios were calculated using a day/night image pair from February 12, 2003.

For the following equations, D is referring to the day image of 2003-02-12, N represents the night acquisition. The subscript reflects the MODIS band number used.

Try 1: second level ratios:

$$Try1_a \equiv \frac{N_{20} / D_{20}}{N_{29} / D_{29}} \quad Try1_b \equiv \frac{N_{20} / D_{20}}{N_{32} / D_{32}} \quad Try1_c \equiv \frac{N_{29} / D_{29}}{N_{32} / D_{32}}$$

Try 2: Subtractions of ratios:

$$Try2_a \equiv N_{20} / D_{20} - N_{29} / D_{29} \quad Try2_b \equiv N_{20} / D_{20} - N_{32} / D_{32} \quad Try2_c \equiv N_{29} / D_{29} - N_{32} / D_{32}$$

Try 3: Ratios of differences:

$$Try3 \equiv \frac{D_{32} - N_{32}}{D_{20} - N_{20}}$$

### 4.5. Maximum vs. Average

During the bowtie correction, the user has the option of overriding the default resample weighting flag from *average* to *maximum*.

*Average* refers to an elliptical weighted averaging of the values during resampling. This method can introduce intermediate output values that do not necessarily appear in the input. However, it produces an anti-aliased output image.

The *maximum* setting entails an elliptical maximum weight sampling. This method is analogous to nearest neighbour sampling in that it will not result in output values that do not appear in the input. However, it can produce aliasing artefacts in the output image

(<http://nsidc.org/PROJECTS/HDFEOS/MS2GT/>).

All images were bowtie corrected with the default setting of averaging the values. To judge if this default setting influences the result of the following analysis, the day and night images of March 18, 2002 were re-processed with the resample weighting setting on maximum.

## 5. Results and Discussion

### 5.1. Brightness Temperature Results

When looking at the brightness temperature images, it becomes very apparent, that solar heating, water surfaces as well as vegetation cover density strongly influence the sensed temperatures. To detect areas that have temperatures above background values, the short TIR wavelengths should be used. With an expected hotspot temperature of 400-500 K, band 20 should reveal higher radiance for fire than for background pixels (compare Blackbody curves in fig. 2), as long as the background temperature stays low enough.

On day time images neither the strongest coal fires in Ruqigou nor the strongest anthropogenic hotspots (e.g. steel industry near Wuda) are visible. Solar heating is too strong; background temperatures rise to a level where hotspots cannot be detected anymore. This holds for summer as well as winter day time images. In the summer scenes, vegetated areas show a strong cooling effect during day time (Figure 4a)

On night time images, the industrial hotspots as well as the hotter coal fires (Ruqigou) can be seen. The contrast between the background values and the fire pixels is still quite low. Especially in the summer image, the eastern flank of the Helan Shan still contains a lot of heat from the sun on this CET 14:45 (i.e. 22:45 local time) image. In this image the Helan Shan still shows up just as bright as the fires in Wuda and brighter than the Ruqigou fires. In winter images, the remaining heat in the rock at acquisition time is considerably less.

Depending on the aspect and steepness of the slope and the thermal inertia of the surrounding rocks, coal fire detection in a single band night time scene will be difficult in winter and impossible in summer.

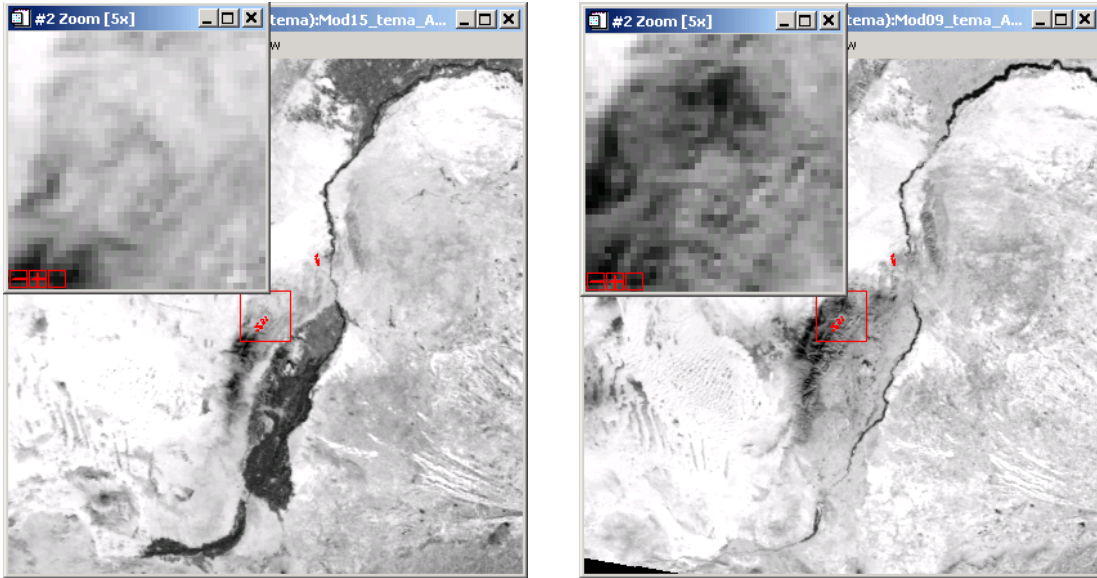


Figure 4 MODIS band 20 day time images; a) summer day time scene of August 29, 2002 with vegetated areas showing up in dark along the Yellow River valley; b) winter day time scene of February 12, 2003. Both images linearly stretched on the zoom window.

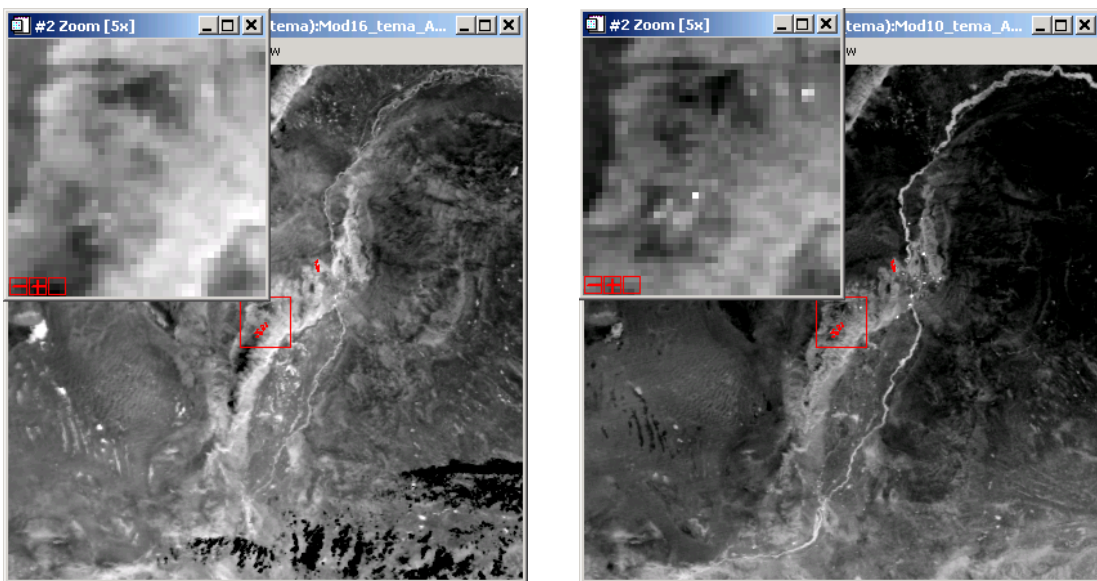


Figure 5 MODIS band 20 night time images; a) summer night time scene of August 29, 2002 with the eastern slopes of the Helan Shan (east of Ruqigou study area) still hot from the day; b) winter night time scene of February 12, 2003. Solar heating effects are still visible but less pronounced than during summer. Both images linearly stretched on the zoom window.

## 5.2. Band Ratioing Results

Bands within a scene were ratioed as described in Chapter 4.2. The resulting night time images show considerably better results than just single band brightness temperature images. The ratioing of bands reduces the effects of warm rocks (thermal inertia), vegetation and water surfaces on the results, while

stressing pixels with two different surface temperatures (fire / background). A summary of the quality of the resulting ratios can be found in Appendix B.

In day time images, the ratioing can still not resolve many of the fires. As the images show below, only the hottest pixel in Ruqigou and some industry hotspots near Wuda show up in the winter day time image. The summer day time images are not useful even when ratios are used.

The band ratio 23/32 appears to give slightly better results in the day time images than the band 20/32 ratio used for night images. The explanation for this behaviour lies probably in the higher amount of reflected solar irradiation in the shorter wavelengths during day time hours.

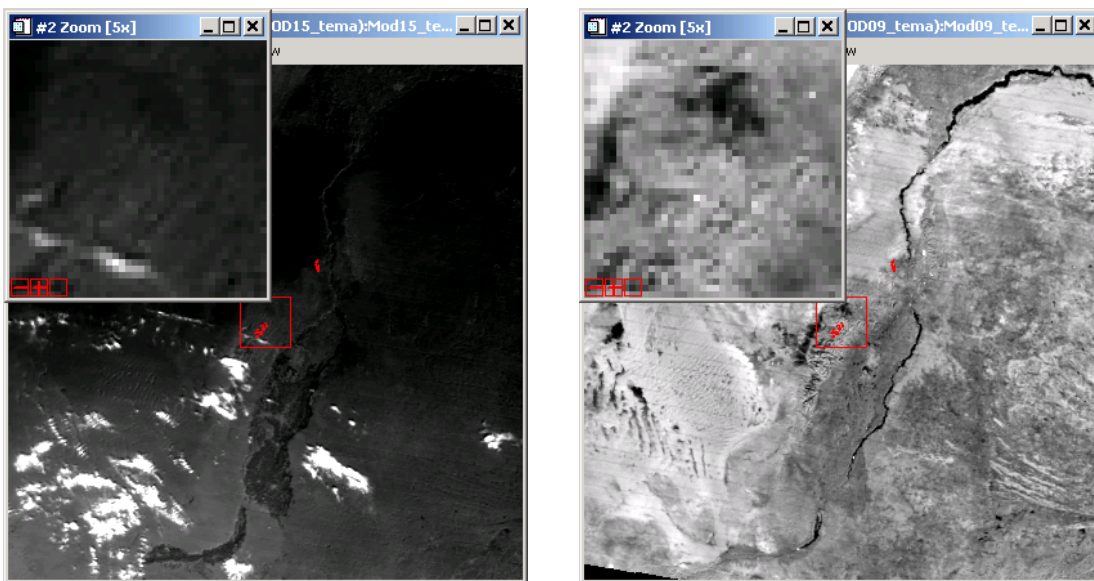


**Figure 6 MODIS band ratio 23/32 day images; a) the summer day time scene of August 29, 2002 shows no results; b) the winter day time scene of February 12, 2003 reveals a hot spot just left below centre and in the top right corner. Both images linearly stretched on the zoom window.**

The best results are achieved using ratios of night time images. As shown in the picture below the ratioing smoothens the background as they show similar brightness temperatures in both bands (especially true in case of winter scenes). The pixels with a mixture of background and fire temperature stand out in the ratios. In all night time cases, band ratio 20/32 gives excellent results. Ratios 22/32 and 24/32 also show reasonable results.

In one winter night image, fires in the Wuda syncline are also visible (Fig 8b). The northern group of bright pixels represents the surface fire in the waste piles just north of the syncline. The southern group of pixels with an increased band ratio comprises of the coal seam fires locally known by their identification number 10, 11, 13 and the south tip of Fire 8. In the 2003 field campaign, this area of the syncline was recorded to contain the biggest surface temperature anomalies. It was also noted, that most fires were burning more intensely in September 2003 than they had been one year earlier. This may also explain why the 2003 image in Fig 8b (acquired February 12, 2003) shows the temperature anomalies in the Wuda syncline much more clearly than the comparable 2002 image in Fig 8a acquired 11 months earlier (March 18, 2002)

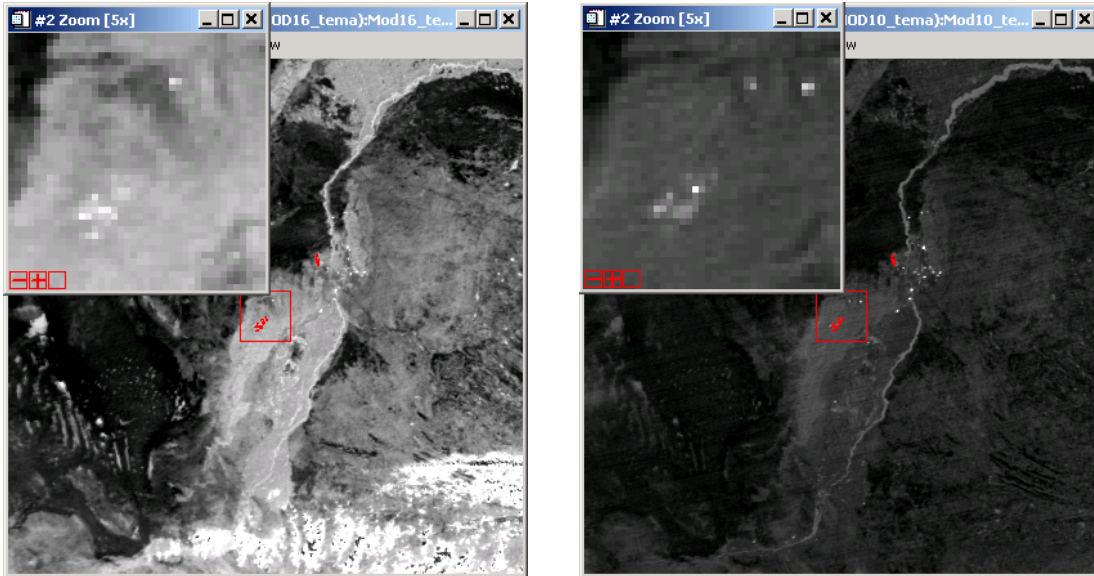


Figure 7 MODIS band ratio 20/32 night images; a) the summer night time scene of August 29, 2002 shows the Ruqigou fires clearly as well as a hot spot in the northeast quadrant of the zoom window; b) the winter night scene of February 12, 2003 shows even better contrasts; other hot spots southeast of Wuda along the Yellow River are heat sources from industry Both images linearly stretched on the zoom window.

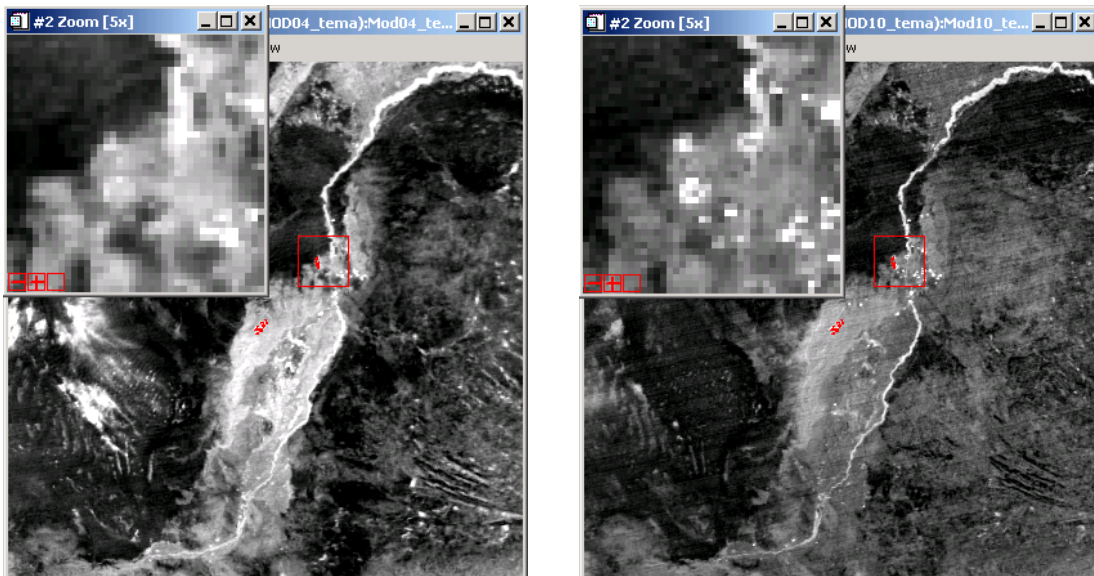


Figure 8 Comparison of MODIS band ratio 20/32 night images; a) winter night scene of March 18, 2002. Distinction between fires and background is difficult; b) the comparable winter night scene of February 12, 2003 clearly shows the fires, industrial hot spots and the Yellow River. Both images 2% linearly stretched on the zoom window

### 5.3. PC and MNF Results

Principle Components and Minimum Noise Fraction Rotations did not reveal promising results.

Components 3, 4, 6, and 9 show some results in one night scene (March 18, 2002). When PC rotation is calculated on the band ratio collection of the same scene, components 1, 5, and 9 reveal some results.

All results shown by PC or MNF rotation methods were always less useful than the band ratios of the same scene. For developing an actual detection method, these rotation methods also show another shortcoming; the outcome of the analysis depends strongly on the overall content of the input scene. Scenes of different areas will use their unique rotation parameters which makes the selection of suitable output components for an unknown monitoring area difficult.

#### 5.4. Day/Night Pair Results

Try1<sub>a</sub> and Try1<sub>b</sub> only show the very hottest industry but none of the coal fire pixels. Try1<sub>c</sub> does not produce any usable results.

Try2 shows similar results as Try1. Try2<sub>a</sub> and Try2<sub>b</sub> show the industrial hotspots. Try2<sub>c</sub> does not produce any usable results.

Try3 shows industrial hotspots quite clearly and gives an idea of raised values for the coal fire areas as well.

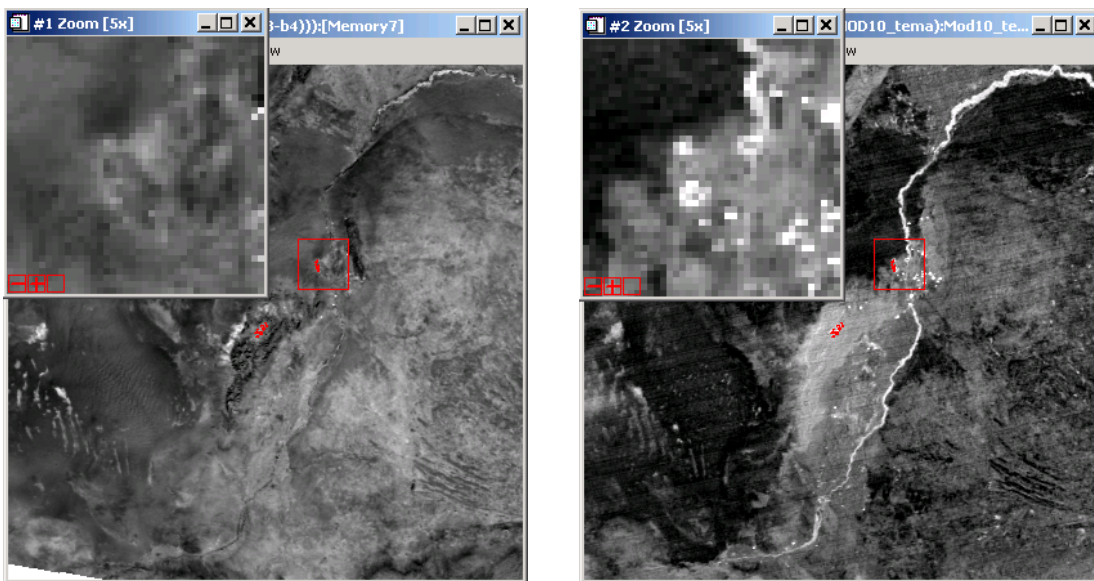


**Figure 9** Comparison of MODIS day/night calculation with a single night scene ratio; a) day/night combination according to formula Try3. Two industrial hot spots are visible along the right edge of the zoom window; b) the 20/32 band ratio of the same days night scene shows the hot spots much clearer. Both images from February 12, 2003 and 2% linearly stretched on the zoom window

Some simple algorithms comparing MODIS day and night images of the same day show small temperature anomalies better than the day images by themselves. However, none of the tested combinations of day and night acquisitions has given us better results than the night images analysed alone (Fig 9a and 9b)

## 5.5. Maximum vs. Average Results

As described in Chapter 4.5, the bowtie correction allows for two types of weighting during the resampling process, average and maximum.

It was observed that the averaging algorithm, especially in areas far from nadir, causes a strong smoothing of the data. On one hand, this will make the background less noisy and the anomalies stand out more. On the other hand, if the anomaly is not very strong, it may also become averaged too much to show up properly.

As we are interested in areas with maximum radiances, the maximum weighting will not make any of the pixels we are interested in drop out.

On the contrary, anomalies may show up in pixels adjacent to actual fire areas. This is caused by the large overlap of the ifovs in scan direction during the acquisition (oversampling) as well as by the overlap of the scan lines in flight direction.

Both effects increase in magnitude with distance from the flight line (i.e. nadir) and are amplified by the biasing maximum weighting.

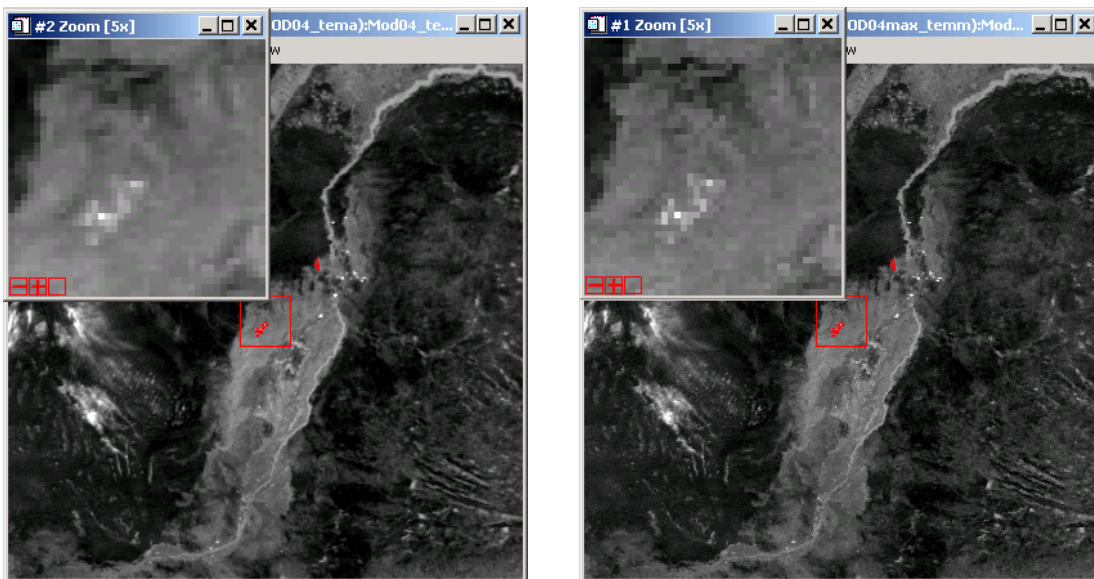


**Figure 10 Comparison of resampling weight setting; a) average weighting smoothens background as well as hot spots; b) maximum weighting gives good detection contrast but may exaggerate the temperature contrast and size of the actual fire area. Both images from March 18, 2002 and linearly stretched on the zoom window**

## 6. Conclusions and Recommendations

Seven day and nine night scenes acquired by the MODIS/Terra sensor were analysed to determine the potential of MODIS/Terra data in the field of coal fire detection and monitoring. Four different types of band manipulations and calculations were tried out to test for increased detectability of these hotspots compared to the originally acquired temperature images.

Of those four manipulations, Principle Components and Minimum Noise Fraction rotations both revealed no real useable results. While some of the industrial hotspots were visible, the coal fires were not. By definition, these methods are also hard to control as rotation parameters change from one scene to the next and the usefulness of the outcome may be hard to predict for a whole region.

Comparing day and night images did not supply us with useable outputs either. Again, some industrial hotspots are visible but for the detection of the coal fires, the contrasts between the fire pixels and the background is not good enough.

As visible in figure 11, using *average* weighting factor for the resampling during the bowtie correction smoothens the output. Although a little more noisy in the background values, the maximum weighting resampling method gives results much richer in contrast and, hence, is preferred.

If brightness temperature images are used without further processing, day time acquisitions are of no use for even the hottest fires. On night time images, fires can be visible in the shortest TIR bands (i.e. MODIS band 20) if the surrounding rocks are cold enough (e.g. winter scenes). It is expected, that pre-sunrise images of the MODIS/Aqua sensor (local overflight time in Wuda ca. 03:00 h) will give slightly better results than the early night MODIS/Terra images (local time ca. 23:00 h) due to remaining heat from the day in the rocks.

Band ratioing of MODIS/Terra images improves the results compared to single band brightness temperatures considerably.

Day time images show weak results; only the hotspots from industrial plants and the most intense coal fire pixels in Ruqigou show up. Best day time band ratio seems to be 23/32.

Night time images show excellent results; the shape of the burning area in Ruqigou is clearly visible in all cloud free images. The fires in Wuda are harder to detect and do not show up properly in most night scenes. An exception is the February 12, 2003 night image (Fig 10b) that also depicts the larger surface anomalies of the Wuda syncline. This difference to other, older scenes is attributed to the increase in fire intensity in the Wuda syncline observed during the 2003 fieldwork.

The best night time band ratio is 20/32, closely followed by 22/32 and 23/32.

The MODIS sensor on Aqua was designed to be identical to the sister sensor on Terra. In this study, we did not deal with MODIS/Aqua data and it is not known to what extent the datasets of the two sensors differ. It might be worthwhile to investigate, if the same band ratios can be applied successfully on MODIS/Aqua data as well.

Since both sensors acquire data for almost the whole world on a daily basis, each spot could be covered twice during the day and twice during the night on almost every day. With most traditionally used earth observing sensors being switched off while on the night side of the orbit, the MODIS instruments are also acquiring during on the dark side of the earth.

It is beyond the scope of this study to develop an actual detection algorithm for MODIS imagery. A statistics-based detection method is currently being developed by J. Zhang / DLR for Landsat 7 ETM+ Band 6 data. It is expected (J. Zhang; personal communication) that the same method can be adjusted to fit MODIS data as well. Results of this detection method are yet to be finalized.

The results above show, that detection and monitoring of coal fire related hotspots with MODIS/Terra imagery is technically possible. Industrial hotspots (e.g. steel factories) are sub-pixel sized thermal anomalies, as are the coal fires. On a simple band ratio suggested in this document, industrial hotspots are not properly distinguishable from coal fire related hotspots. Since coal fires can range from just above background temperature to many hundred Kelvin (large surface fire), they also cover a similar temperature range as industrial plants do. This prevents separation of the two types of hotspots via Dozier's two temperature linear mixing model (Dozier, 1981).

With a 55° scan angle to either side, pixels near the edge of the swath become very large (about 2x5 km). If enough cloud free MODIS night scenes are available, it is recommended to use only the pixels up to a maximum scan angle (e.g. 30° => 1.4x1.2 km maximum pixel size ).

## 7. Acknowledgements

This research was carried out as part of the DLR / ITC coal fire research collaboration effort under the umbrella of the project titled: "*Reception and project specific processing of remote sensing data for the support of current and future projects within the Chinese-German environmental research co-operation*"

I would like to thank Anke Tetzlaff, DFD-DLR for the scientific exchange and support.

Harald van der Werff, ITC helped with LINUX related issues. Thanks for your speedy assistance.

Jeanna Hyde Hecker, ITC gave valuable comments on a draft version of this report.

## 8. References

- Dozier, J. (1981). A method for satellite identification of surface temperature fields of subpixel resolution. *Remote Sensing of Environment*, 11, 221-229.
- Rosema, A., Guan, H., Veld, H., Vekerdy, Z., Ten Katen, A. M., & Prakash, A. (1999). *Manual of Coal Fire Detection and Monitoring* (NITG 99-221-C): Netherlands Institute of Applied Geosciences.
- Zhang, J., Wagner, W., Prakash, A., Mehl, H., & Voigt, S. (2003). Review Article: Detecting coal fires using remote sensing techniques. *International Journal of Remote Sensing*, in print.

## 9. Appendices

## 9.1. Appendix A

Inventory of downloaded MODIS scenes

Scene_Code	Date	Time	dn	relative2Nadir	MOD 021KM	MOD 02HKM	MOD 02QKM	MOD 02OBC	MOD 03	MOD 05_L2	MOD 11_L2	MOD 14	MOD 35_L2	Alternative Scene Code	Conditions_AOI
2001266.1515	2001_09_23	15:15h		slight east	x				x					Mod01	Wuda partly cloudy; Ruq cloudy
2001275.1510	2001_10_02	15:10h		centred	x				x	x	x	x	x	Mod02	partly cloudy? Maybe Snow??
2002077.0405	2002_03_18	4:05d		medium east	x	x			x	x	x	x	x	Mod03	excellent
2002077.1510	2002_03_18	15:10h		medium east	x	x			x	x	x	x	x	Mod04	excellent
2002117.1420	2002_04_27	14:20h		med-far west	x				x					Mod05	not usable; problems with georef?? (Wuda cloudy; Ruq OK)
2002239.0355	2002_08_27	3:55d		slight east	x				x	x	x	x	x	Mod13	good but small clouds over Ruqigou area
2002239.1500	2002_08_27	15:00h		centred	x				x	x	x	x	x	Mod14	clouds bordering both AOIs; maybe useful for masking try-outs
2002241.0340	2002_08_29	3:40d		slight west	x				x	x	x	x	x	Mod15	excellent
2002241.1445	2002_08_29	14:45h		medium west	x				x	x	x	x	x	Mod16	excellent
2002344.0345	2002_12_10	3:45d		centred	x				x	x	x	x	x	Mod06	excellent
2002344.0350	2002_12_10	3:50d		centred	x				x	x	x	x	x	Mod07	excellent; AOI slightly outside scene
2002344.1450	2002_12_10	14:50h		slight west	x				x	x	x	x	x	Mod08	good; some haze SE of AOI
2003043.0345	2003_02_12	3:45d		slight west	x				x	x	x	x	x	Mod09	excellent
2003043.1450	2003_02_12	14:50h		centred	x				x	x	x	x	x	Mod10	excellent
2003044.0430	2003_02_13	4:30d		far east	x				x					Mod11	good; some haze S, E and W of AOI
2003044.1535	2003_02_13	15:35h		far east	x				x					Mod12	not usable

## 9.2. Appendix B

Table of Band ratios and assessment of visibility of known fire locations

	Mod01	Mod02	Mod03	Mod04	Mod05	Mod06_07	Mod08	Mod09	Mod10	Mod11	Mod12	MOD13	MOD14	MOD15	MOD16	Mod03max	Mod04max
Ruigou	Cloudy	clearly	no	clearly	cloudy	little	clearly	no	clearly	Cloud/snow	clouds/snow	no	clouds	no	clearly	no	clearly
20_32		clearly	no	clearly	cloudy	little	clearly	no	clearly	Cloud/snow	clouds/snow	no	clouds	no	clearly	no	clearly
20_31		clearly	no	clearly	cloudy	little	clearly	no	clearly	Cloud/snow	clouds/snow	no	clouds	no	clearly	no	clearly
20_29		yes	no	clearly	cloudy	no	yes	no	yes		little	no		no	clearly	no	clearly
23_32		little	no	yes		little	yes	little	yes		little	no		no	yes	no	yes
23_29		little	no	yes		little	yes	no	yes		little	no		no	yes	no	yes
22_32		yes	no	yes		little	yes	little	yes		little	no		no	yes	no	yes
22_29		yes	no	yes		no	yes	no	yes		little	no		no	yes	no	yes
20_22		little	no	little		no	little	no	little			no		no	little	no	little
20_23		little	no	little		no	little	no	little			no		no	yes	no	little
32_31		no	no	no		no	no	no	no			no		no	no	no	no
32_29		no	no	no		no	no	no	no			no		no	no	no	no
20_34		little	no	little		no	little	no	little			no		no	little	no	little
20_35		little	no	little		no	little	no	little			no		no	little	no	little
Wuda	cloudy	little	no	little	cloudy	no	clearly	no	clearly	no	clouds	no	clouds	no	little	no	little
20_32		little	no	little	cloudy	no	clearly	no	clearly	no	clouds	no	clouds	no	little	no	little
20_31		little	no	little		no	clearly	no	clearly	no		no		no	little	no	little
20_29		no	no	no		no	clearly	no	clearly	no		no		no	no	no	no
23_32		no	no	little		no	yes	no	yes	no		no		no	little	no	little
23_29		no	no	no		no	little	no	little	no		no		no	no	no	no
22_32		little	no	little		no	yes	no	yes	no		no		no	little	no	little
22_29		no	no	no		no	yes	no	yes	no		no		no	no	no	no
20_22		no	no	no		no	little	no	little	no		no		no	no	no	no
20_23		little	no	no		no	little	no	little	no		no		no	no	no	no
32_31		no	no	no		no	no	no	no	no		no		no	no	no	no
32_29		no	no	no		no	no	no	no	no		no		no	no	no	no
20_34		little	no	little		no	little	no	little	no		no		no	little	no	little
20_35		little	no	little		no	little	no	little	no		no		no	little	no	little

Fire visibility categories clearly yes little no  
 For explanation of alternative scene codes consult Appendix A

### 9.3. Appendix C

Content of parameter files used in bowtie correction  
(underlined XX to be replaced by file name)

#### Ancilfile.txt

```
seze scaled
soze scaled
```

#### Bowtie\_ModXX.sh

Shell file to start operation

```
mod02.pl . MODXX listfile.txt Ninxia.gpd chanfile.txt ancilfile.txt 3 3
```

#### Chanfile.txt

```
20 temperature
21 temperature
22 temperature
23 temperature
24 temperature
25 temperature
27 temperature
28 temperature
29 temperature
30 temperature
31 temperature
32 temperature
33 temperature
34 temperature
35 temperature
36 temperature
```

#### Listfile.txt

```
MOD021KM.XX...XX.hdf
```

#### Ninxia.gpd

```
Ninxia.mpp map projection parameters #
```

```

800 600          columns rows          # area around Yinchuan w/
Wuda and Ruqigou
10              grid cells per map unit  # 1 km cells
400  300  map origin column,row
    
```

### **Ninxia.mpp**

```

Azimuthal Equal-Area
39.0 106.0  lat0 lon0
0.0          rotation
10.0         scale (km/map unit)
39.0 106.00  center lat lon
0.00  90.00  lat min max
-180.00 180.00 lon min max
15.00 30.00 grid
0.00  00.00 label lat lon
1 0 0      cil bdy riv
    
```

## 9.4. Appendix D

LINUX shells and source codes

### Ms2gt\_env.sh

Shell file to set environmental parameters / paths for rest of bowtie processing

Execute right after logon with “source ms2gt\_env.sh”

```

#!/bin/bash
#
# Bash script to set environment for ms2gt
#
# Only MS2GT_HOME and IDL_DIR should normally need adjustments,
# other variables are defaults of ms2gt.
#
# Harald van der Werff, ITC, 2003

# Set ms2gt variables and path

export MS2GT_HOME=$HOME/tutorial1_plus_data/ms2gt

export PATH_MS2GT_SRC=$MS2GT_HOME/src
export PATH_MS2GT_IDL=$PATH_MS2GT_SRC/idl
export PATH="$MS2GT_HOME/bin:$MS2GT_HOME/src/scripts:$PATH"

# Set initial values for $IDL_DIR, $IDL_PATH, and $PATHMPP if they aren't
yet defined

if [ ! $IDL_DIR ]; then
    export IDL_DIR="/usr/local/rsi/idl"
fi
if [ ! $IDL_PATH ]; then
    export IDL_PATH="\+$IDL_DIR/lib"
fi
export IDL_PATH=$IDL_PATH\:\+$PATH_MS2GT_IDL

if [ ! $PATHMPP ]; then
    export PATHMPP="."
fi
export PATHMPP=$PATHMPP\:$MS2GT_HOME/grids

```

### Chris.java

Source code to create an ENVI readable Control Pont File from the MS2GT geolocation output files (reads lat and long from two separate floating point files and combines the columns with row and col counters).

File was compiles through <compile.sh>

```

/**
 * chris.java
 *
 * @author Harald van der Werff

```

```
*/

import java.io.BufferedReader;
import java.io.File;
import java.io.FileNotFoundException;
import java.io.FileReader;
import java.io.IOException;
import java.util.StringTokenizer;
import java.util.Vector;

public class Chris {
    private float[][] firstArray, secondArray;
    //private BufferedReader fileReader;
    private Vector rows, cols;
    private int numRows, numCols;

    public static void output(String text) {
        /** Handles screen output */
        System.out.println(text);
    }

    public static void error(String errorString) {
        /** Handles error messages */
        System.out.println(" ");
        System.out.println(errorString);
        System.out.println("Exiting...");
        System.out.println(" ");
        System.exit(1);
    }

    public static void showHelp() {
        /** Handles help on argument errors*/
        output("");
        output("Usage: java chris [1st filename] [2nd filename]");
        output("");
        output("increase memory: java -Xms64m -Xmx250m ...");
        output("");
        System.exit(1);
    }

    public void checkFile(String fileName) {
        /** Quick check if files exist */
        File testFile = new File(fileName);
        if ( ! testFile.exists())
            error(" " + fileName + ": failing");
    }

    public float[][] readArray(String fileName) {
        /** read input file, put data into array */
        File file = new File(fileName);
        try {
            BufferedReader fileReader = new BufferedReader(new Fil-
eReader(file));
            rows = new Vector();
            cols = new Vector();
            try {
                String line = fileReader.readLine();
                while (line != null) {
```

```

        if (!line.startsWith(";")) {
            StringTokenizer dataToken = new StringToken-
izer(line);

            cols = new Vector();
            while (dataToken.hasMoreTokens()) {
                try {
                    cols.add(new
Float(Float.parseFloat(dataToken.nextToken())));
                } catch (NumberFormatException nfe) {
                    error("Could not parse float from
file" + fileName);
                }
            }
            rows.add(cols);
        }
        line = fileReader.readLine();
    }

    } catch (NumberFormatException nfe) {
        output("Could not read from file" + fileName);
    }
    fileReader.close();
} catch (IOException nfe) {
    output("could not open file" + fileName);
}
numRows = (rows.size() -1);
cols = (Vector) rows.elementAt(0);
numCols = cols.size();
//numCols = 800;
float[][] array = new float[numRows][numCols];
for (int i = 0; i < numRows; i++) {
    cols = (Vector) rows.elementAt(i);
    for (int j = 0; j < numCols; j++) {
        array[i][j] = ((Float)
cols.elementAt(j)).floatValue();
        //output("array: " + array[i][j]);
    }
}
return array;
}

public void writeArray(float[][] firstArray, float[][] secondArray) {
    /** writes output array to screen **/
    for (int i=0; i < numRows; i++) {
        for (int j=0; j < numCols; j++) {
            output(firstArray[i][j] + " " + secondArray[i][j] + " " +
(j+1) + " " +
                (i+1) );
        }
    }
}

public void Chris(String firstFileName, String secondFileName) {
    firstArray = readArray(firstFileName);
    secondArray = readArray(secondFileName);

    writeArray(firstArray, secondArray);
}

```

```
public static void main(String[] args) {
    /** main program*/

    if (args.length != 2) {
        showHelp();
    }

    String firstFileName = " ";
    String secondFileName = " ";

    firstFileName = args[0];
    File firstFile = new File(firstFileName);
    if ( ! firstFile.exists())
        error(firstFileName + " is failing");

    secondFileName = args[1];
    File secondFile = new File(secondFileName);
    if ( ! secondFile.exists())
        error(secondFileName + " is failing");

    Chris i = new Chris();
    i.Chris(firstFileName, secondFileName);
}
```

### Compile.sh

```
#!/bin/bash
#
# Shell script to compile Java source code
#
# Arko Lucieer
# August 10, 2001
# Edited by Harald van der Werff
# September 25, 2002
#
export CLASSPATH=.:$CLASSPATH
echo Compiling...
javac -d . Chris.java
echo Finished...
```

### Chris.sh

Shell file to start the chris executable.

Usage: "chris.sh longitudefilename latitudefilename > outputfilename"

```
#!/bin/bash
java -Xms64m -Xmx350m -classpath /home/hecker/bin Chris $1 $2
```